Fluctuation analysis of activity biosensor images for the study of information flow in signaling pathways

Marco Vilela[1], **Nadia Halidi**[1], **Sebastien Besson**[1], **Hunter Elliott**[1], **Klaus Hahn**[2], **Jessica Tytell**[1], and **Gaudenz Danuser**[1]

Marco Vilela: Marco_Vilela@hms.harvard.edu; Nadia Halidi: Nadia_Halidi@hms.harvard.edu; Sebastien Besson: Sebastien_Besson@hms.harvard.edu; Hunter Elliott: Hunter_Elliott@hms.harvard.edu; Klaus Hahn: khahn@med.unc.edu; Jessica Tytell: Jessica_Tytell@hms.harvard.edu; Gaudenz Danuser: Gaudenz_Danuser@hms.harvard.edu

[1]Department of Cell Biology, Harvard Medical School, Boston, Massachusetts 02115, USA

[2]Department of Pharmacology and Lineberger Cancer Center, University of North Carolina at Chapel Hill, Chapel Hill, North Carolina 27599, USA

Abstract

Comprehensive understanding of cellular signal transduction requires accurate measurement of the information flow in molecular pathways. In the past, information flow has been inferred primarily from genetic or protein-protein interactions. Although useful for overall signaling, these approaches are limited in that they typically average over populations of cells. Single cell data of signaling states are emerging, but these data are usually snapshots of a particular time point or limited to averaging over a whole cell. However, many signaling pathways are activated only transiently in specific subcellular regions. Protein activity biosensors allow measurement of the spatiotemporal activation of signaling molecules in living cells. These data contain highly complex, dynamic information that can be parsed out in time and space and compared with other signaling events as well as changes in cell structure and morphology. We describe in this chapter the use of computational tools to correct, extract, and process information from timelapse images of biosensors. These computational tools allow one to explore the biosensor signals in a multiplexed approach in order to reconstruct the sequence of signaling events and consequently the topology of the underlying pathway. The extraction of this information, dynamics and topology, provides insight into how the inputs of a signaling network are translated into its biochemical or mechanical outputs.

Keywords

biosensor; FRET; image analysis; correlation; information flow; signal transduction

1. Introduction

Optical microscopy has been widely applied to study the dynamics of molecules in biological systems. Accompanied by the development of fluorescently-tagged proteins,

Correspondence to: Gaudenz Danuser, Gaudenz_Danuser@hms.harvard.edu.

microscopy can provide insightful information about not only the state of single cells, but also subcellular variation in protein concentration and dynamics (Slavík, 1996). For instance, Fluorescence Speckle Microscopy (FSM) has been used to track directly protein motion and aggregation in supra-molecular structures (Waterman-Storer et al., 1998). Alternatively, Fluorescence Correlation Spectroscopy (FCS) characterizes protein dynamics by statistical analysis of intensity fluctuations measured within a small volume (Schwille and Haustein, 2009). This method has been used to quantify the motion and interaction of diffusing proteins and organelles (Digman and Gratton, 2011). There are many different microscopy techniques designed to approach a wide variety biological questions and we refer to (Goldman et al., 2010) for a complete description.

Although very informative, canonical microscopy techniques are limited to report only local variations of protein concentration. However, the functionality of many proteins depends not only on concentration but also on the protein's activation state. For instance, members of the small GTPases family of proteins are only active when bound to the nucleotide GTP and become inactive when GTP is hydrolyzed to GDP (Raftopoulou and Hall, 2004). A considerable amount of research has been done in the past decade to include the state of molecular activity as an experimental readout. This effort led to the development of fluorescent constructs that report protein activation in living cells, which are referred to here as 'activity biosensors' or simply 'biosensors' (Newman et al., 2011; VanEngelenburg and Palmer, 2008). The sensitivity of biosensors is often sufficient to resolve subcellular variations in the activation state, even with mild, physiologically relevant stimulation of pathways or with changes due solely to endogenous fluctuations. Therefore, unlike standard fluorescent protein tagging strategies, biosensors can track the spatiotemporal propagation of signals within a cell rather than just the redistribution of protein molecules (Figure 1).

The goal of this chapter is to illustrate the steps necessary to acquire time-lapse image sequences of biosensors and to derive the **information flow** in signaling pathways from the spatiotemporal variations of the sensor's activation. The information flow defines both the topology of signal transduction and the activation kinetics. Importantly, information flow is a generic concept that captures not only the activation and/or transport of signaling molecules as illustrated in Fig. 1, but also morphological events like the assembly and disassembly of supra-molecular structures, the motion of a particular subcellular region, or force generation. One of the key strengths of studying information flow is that it does not require a direct link between the observed components. Sampled components may be linked by several unobserved and potentially unknown intermediates, and yet, their relationships can still be inferred. Therefore, measuring information flow provides a general means to establish the organization of cellular signal transduction pathways, even when knowledge or observations of the network components are incomplete.

2. Activity biosensors

2.1 Types of activity biosensors

The term "biosensor" has been applied to a wide range of imaging probes that detect localization and/or activation of a particular molecule. Many of them are irreversible in measuring the activation or deactivation of a molecule, making them unsuitable for the

analysis of information flows in signaling pathways. To deduce information flows, biosensors must report changes in the activation state of a molecule in both directions, from an inactive to an active state and vice versa. Therefore, for the remainder of the chapter we will focus only on this class of biosensors..

Many activity biosensors share a common design scheme in which an "affinity reagent" that binds only to the active form of the probed signaling molecule is coupled to a "readout module" which changes its optical properties, most often its fluorescence, in response to binding or unbinding of the affinity reagent. Activity biosensors can be divided into two broad categories. The first category, perhaps the most common, uses protein-based affinity reagents and readout modules. These are genetically encoded biosensors in which protein-based fluorophores are incorporated such that binding between the affinity reagent and the target affects fluorescent properties, usually FRET (Periasamy, 2001). FRET is an excellent readout for biosensors because small changes in the distance or orientation between the two fluorophores can cause large changes in FRET efficiency, allowing sensitive detection of protein binding or conformational changes. For example, one member of the FLARE (**Fl**uorescence **A**ctivation **Re**porter) family of Rho GTPase sensors (Hodgson et al., 2008) consists of the RhoA protein fused to a CFP-donor followed by a YFP acceptor fluorophore and finally the RhoA-binding domain (RBD) of the RhoA effector molecule Rhotekin, all in a single protein (Pertz et al., 2006). As RhoA is activated by binding to GTP, it undergoes a conformational change that increases its affinity for the RBD. RBD-binding then folds the sensor so that the two intermediary CFP and YFP fluorophores are brought into close proximity, resulting in a heightened FRET efficiency. Many biosensors of this class with similar design principles have been designed over the past 10 years to monitor the activity of a wide class of molecules. We refer to reviews such as (Newman et al., 2011; VanEngelenburg and Palmer, 2008) for comprehensive tables and descriptions of these sensors.

The second category of activity biosensor uses a hybrid design where the affinity reagent is a protein but the readout module is an environmentally sensitive dye. For these biosensors, the dye is ligated to the protein domain in a region where binding of the activated molecule of interest alters the local solvent environment near the dye, thereby altering the dye's fluorescent properties. These sensors can be significantly brighter than their fluorescent protein relatives, and report activation of endogenous proteins, but they can must be mechanically loaded (ie via microinjection, electroporation etc), which limits the number and type of cells that one can image. One example of this type of biosensor is a Cdc42 biosensor using a domain of WASP, a Cdc42 interacting protein that binds selectively to the activated (GTP-bound) Cdc42 but not other closely related GTPases (Abdul-Manan et al., 1999; Nalbant et al., 2004). This domain was used as the affinity reagent and an environmentally-sensitive merocyanine dye was fused to this domain. When the sensor binds to endogenous Cdc42, the solvent environment of the merocyanine dye changes. This leads to increased fluorescence intensity at a particular wavelength. To distinguish activity-associated changes in intensity from changes in localization the affinity reagent is fused with a second tag, in the of the Cdc42 biosensor a GFP, serving as a reference signal for ratiometric analyses (see below).

2.2 Design of the affinity reagent

One of the most important aspects of biosensor design is the selection of the affinity reagent. The key attribute of the affinity reagent is that it must recognize an inter- or intra-molecular change in structure or binding caused by activation of the molecule of interest. Most biosensors are produced using rational design methods where candidate affinity reagents are based on known binding partners. For example, for the Cdc42 and RhoA biosensors, the affinity reagent was based on effector proteins known to specifically bind to the active form of the respective GTPase. As another example, in the Perceval ATP/ADP sensor (Berg et al., 2009), a circularly permuted mVenus is connected to a portion of a protein, GlnK1, that changes structure upon ATP binding. In this case ATP or ADP binding to the GlnK1 domain differentially alters the mVenus structure leading to measurable changes in fluorescence at different wavelengths. Most recently, affinity reagents have been developed by high throughput screening of fixed biosensor scaffolds, conferring binding affinity for otherwise intractable targets.

2.3 Practical considerations

Ideally a biosensor should have no effect on cellular processes and behavior. However, most biosensors interact with endogenous signaling molecules and, because of this interaction, high levels of biosensor expression can interfere with endogenous signaling through participation in endogenous signaling process and by sequestering signaling molecules or cofactors. It is therefore important to keep biosensor probe levels as low as possible to minimize these perturbations. The behavior of cells containing biosensor should always be compared to the behavior of cells that are not treated or contain a mock biosensor without interacting domains (*e.g.* CFP alone). To obtain sufficient signal from cells expressing low levels of the biosensor, light collection must be maximized. However, care must be taken not to increase irradiation to the level where the biosensor bleaches or to where increased phototoxicity becomes significant. There are several approaches to reduce both photobleaching and phototoxicity; including use of neutral density filters and/or long exposure times, rather than short excitation with intense irradiation, as well as the use of enzyme systems that efficiently scavenge free oxygen in the medium to prevent damage from free radical formation (*e.g.*, oxyfluor, Oxyrase Inc.)

When imaging the spatiotemporal dynamics of a FRET-biosensor, one has to consider the low dynamic range of activation. FRET-based sensors generally measure binary changes (inactive vs. active) between a low and a high FRET state. The difference between the two states varies widely between sensors and can be small. Thus, it is important to determine the differences in the acceptor-to-donor emission ratios between the active and inactive states in order to establish the relevant activation range of a biosensor. To accomplish this, the biosensor construct should be mutated (creating dominant-negative or dominant-positive mutants) in order to determine the minimum and maximum FRET signals in a native cellular environment.

2.4 Image acquisition and data processing

While many methods exist for measuring FRET efficiency in FRET-based biosensors, the most common involves acquiring raw localization and activation images. These images are

then processed into a ratiometric image that indicates the local fraction of active and total amount of signaling protein. This method is referred to as "sensitized FRET" (Periasamy, 2001). When using a CFP as donor and YFP as an acceptor fluorophore, images from three channels are recorded: CFP excitation with CFP emission (donor localization image), CFP excitation with YFP emission (FRET; activation image), and YFP excitation with YFP emission (acceptor localization image). Ideally, images should be captured simultaneously to avoid artifacts caused by cell movement in between frames. However, depending on the rate of change of the activity being measured and the morphodynamic activity of the cell, they can be captured sequentially.

Measurement of FRET efficiency via ratiometric analysis relies on the differences between the localization and activation images, which are frequently subtle. This requires that any other potential differences between these images be removed prior to calculating the ratio image. Therefore, several corrections are required, and they are specific to the imaging system used to collect the raw data. The first two corrections are termed dark current and shade corrections, and they ensure that the measured spatial variations in image intensities are accurate within each image and comparable across the different image channels. Dark current noise refers to activation of the image sensor independent of incident light, which can show significant spatial variation depending on the camera. The shade correction compensates for the non-homogeneous illumination of the sample, which typically declines in a smooth gradient from the center to the edge of the illuminated field. Background subtraction and photobleach corrections ensure that the measured intensities are comparable over time and across experiments at the whole-image level. Background subtraction corrects for differences in spatially uniform, non-biosensor derived image intensities such as media autofluorescence, over which the biosensor image intensities are superimposed. Photobleach correction adjusts for the changes in fluorescence intensities over time associated with the bleaching of either donor or acceptor. Finally, spectral overlap and imperfect spectral filters cause 'bleed-through' between the donor localization image and the acceptor localization image and the activation image, respectively. Bleed-through corrections therefore produce fully independent activation and localization images. These are typically not used for biosensors in which all components are combined in a single chain.

Our lab provides a software package that implements these corrections (download from lccb.hms.harvard.edu). The workflow of the software is shown in Figure 2. It is also possible in this package to correct for image misalignments associated with chromatic aberration and/or mechanical shifts between different cameras (transformation step in Figure 2). Further details can be found in the online documentation and in (Hodgson et al., 2008; Machacek et al., 2009).

3. Extracting activity fluctuations in a cell-shape invariant space

Many signaling pathways are highly regulated and compartmentalized. Moreover, the same signaling protein can be involved in different pathways at different cellular locations. For instance, the small GTPase Rac1 promotes actin polymerization through the recruitment of actin nucleators in cell lamellipodia while it also regulates focal adhesion maturation just few microns away from the actin nucleation sites (Burridge and Wennerberg, 2004). In order

to understand such differences in regulation, signaling events need to be probed with a resolution that matches the spatial variability.

To locally probe signals in living cells we propose an *in silico* compartmentalization of the cell area that is adaptive to cell shape changes (Lim et al., 2010; Machacek and Danuser, 2006; Machacek et al., 2009). Using time-lapse image sequences of cells containing activity biosensors, the cell perimeter is segmented into sampling windows (See Figure 3A) in each of which the local signaling activity is determined by averaging the biosensor readout over all its pixels. The segmentation is performed in all frames of the sequence. Therefore, each window gives rise to a time series that represents the **local fluctuation in biosensor signal**.

A major challenge in implementing the windowing strategy is to match corresponding windows from one frame to the next. This is an important requirement because the time series extracted from one window should represent signal fluctuations of a unique cellular region. This prerequisite becomes difficult to satisfy when the cell undergoes significant changes in morphology, either by changing the cell edge shape or the total area. Different solutions to this problem have been proposed (Bosgraaf et al., 2009; Tyson et al., 2010). Our lab has focused on studies of the connection between the spatiotemporal organization of signaling activities and cell morphological outputs like protrusion, retraction, and migration. Therefore, we developed a strategy for the definition of a cell-shape invariant window mesh – that is, an *in silico* compartmentalization which can be applied irrespective of cell shape or shape changes. After identifying and tracking the local motion of the cell edge, the sampling windows at the cell border follow the frame-to-frame edge displacement. The sampling windows in the cell interior are then constructed relative to these windows in a manner which maintains a fixed relationship to the cell edge. For subsequent processing of the signaling fluctuations the sampled image values are mapped window by window, time point by time point into an activity map (Figure 3B). Importantly, this mathematical representation of image variables is independent of cell shape – cell-shape invariant - allowing comparison of signaling patterns between cells with distinct morphologies. Moreover, in experiments where multiple image variables are acquired, such as simultaneous imaging of multiple biosensors, this mapping enables the analysis of the spatial and temporal relations between variables by correlation methods (described below). Using this approach we have recently explored the relationships between cell morphodynamics and the underlying forces, cytoskeleton dynamics and regulatory signaling (Ji et al., 2008; Lim et al., 2010; Machacek et al., 2009).

Knowledge of the spatial scale of signaling and morphodynamic events is crucial for a meaningful definition of sampling window size. If the window size is too large relative to the spatial variation of the sampled signals, significant fluctuations will be averaged out. If the window size is too small, the readout may be too noisy and neighboring windows may measure the same signaling event. Both issues prevent meaningful analysis of signaling dynamics via fluctuation series. A practical tool to define the window size is the spatial autocorrelation of the activity map (Welch et al., 2011). The autocorrelation can be interpreted as a measure of self-similarity, and is discussed in detail below. By choosing the full width at the half maximum of the spatial autocorrelation as the window size the windows offer a practical compromise between spatial resolution, noise and self-similarity.

4. Correlation analysis of activity fluctuations for pathway reconstruction

This section describes a set of statistical techniques that can be applied to time series data generated from a biosensor movie that has been processed and sampled by the methods described above. The goal of this analysis is to determine correlations, time delays and spatiotemporal scales of the sampled signals with the ultimate goal of piecing together the sequence of signaling events in a pathway.

4.1 Defining the spatiotemporal scale of events

The length and time scales at which signaling events occur are not only biologically meaningful, but are important factors in defining the parameters of data acquisition and data analysis. As discussed above, the spatial scale of signal variations determines the appropriate window size to be used for the sampling of activity maps. Analogously, the temporal scale of signaling variations dictates the frame rate at which biosensor movies must be acquired. Both the spatial and temporal scales are *a priori* unknown properties of the studied pathway. Here we introduce autocorrelation and power spectrum as two methods for determining these scales and for ensuring compliance of the experimental setup and data analysis with the Nyquist theorem. The Nyquist theorem asserts that a continuous, noise-free signal has to be sampled with a rate greater than twice the fastest frequency present in the signal in order to fully reconstruct the original signal (Brigham, 1988). Although conceptually simple, the theorem has important practical implications for experimental design. For instance, Ptk1 cells exhibit a protrusion/retraction cycle with a period of ~130 seconds (Tkachenko et al., 2011). Converted into a frequency, this yields 0.008 cycles per second, or 8 miliHertz (mHz). However, these long cycles may be superimposed by faster switches between protrusion and retraction that occur every ~40 seconds (25 mHz). According to the Nyquist theorem, one would therefore need to acquire an image faster than every 20 seconds (50 mHz) to capture the processes that produce both slow/long and fast/ short edge movements. In practice, sampling at the Nyquist frequency will not be sufficient for a meaningful analysis because of the measurement noise present in the signal. As a rule of thumb, the sampling should be at least twice the Nyquist frequency. Thus, in the example of PtK1 cell protrusions movies have to be acquired with frame rates of 10 seconds or faster.

4.1.1 Autocorrelation—The autocorrelation function (ACF) defines how data points in a time series are related, on average, to the preceding data points (Box et al., 1994). In other words, it measures the self-similarity of the signal over different delay times. Accordingly, the ACF is a function of the delay or lag τ, which determines the time shift taken into the past to estimate the similarity between data points. For instance, in a structured process where nearby measurements have similar values but distant points have no relation, the autocorrelation decreases as the lag τ increases. Conversely, the autocorrelation of an unstructured processes like white noise is, in theory, equal to zero for all values of $\tau > 0$ because there is no effect from one time point on another. This fact is exploited to determine the significance of the autocorrelation values. This significance can be estimated by comparing the autocorrelation of a given time series *X* with the standard error of the autocorrelation of a white noise with the same variance and number of points as that in *X*. A value is considered significant if its magnitude exceeds the standard error of the white noise

(Box et al., 1994). A positive autocorrelation value for a particular lag τ can be interpreted as a measure of persistence of data points separated by this lag to stay above and/or below the mean value of the signal. A negative autocorrelation indicates that data points separated by this lag tend to alternate about the mean value. An important piece of information provided by the ACF is the maximum lag τ_{max} that still has a significant value. This lag indicates the "memory" or temporal persistence of the fluctuation series. Data points separated by time lags greater than τ_{max} are completely uncoupled. The ACF is often redundantly plotted for positive and negative values of τ, although by definition it is symmetric about $\tau=0$. Of note, the ACF can also be computed in space. In spatial autocorrelation the lag τ is then interpreted as a distance between data points. In either case the characteristics of the temporal and spatial autocorrelation of a signaling process help us to understand the scale at which the pathway operates. These scales help us to define appropriate sampling, and provide information on the spatiotemporal characteristics of the associated signal transduction network.

4.1.2 Power Spectrum—The spatial and temporal scales at which cellular signaling operates can be further dissected by analyzing the power spectrum of extracted time-series. The power spectrum measures how the variance of a time series is distributed over different frequencies (Box et al., 1994). The interpretation of the power spectrum is linked to the definition of Fourier series, which describe a signal as a sum of sine and cosine waves with different frequencies and amplitudes (Brigham, 1988). In this sum, each pair of sine and cosine waves with a given frequency ω has a specific amplitude. The power spectrum delineates the amplitudes for all sampled frequencies ω, giving a measure of the contribution of each particular frequency to the net temporal behavior of the signaling system. In practice, the power spectrum is calculated from an averaging process. The signal is split into *N* overlapping windows, Fourier transformed and the amplitude values in each frequency are averaged over all windows to create a global power spectrum density. This averaging process corrects for the fact that the variance of the spectrum increases with the number of points if the entire signal is used as one window. Additionally, it also provides the confidence interval based on the standard deviation calculated from all the overlapping windows (Brillinger and Krishnaiah, 1983). The power spectrum is closely related to the ACF, and in fact can be mathematically defined as the Fourier transform of the autocorrelation function. Like the ACF, the power spectrum is symmetric about the y-axis. We discuss below the relationship between the ACF, power spectrum and temporal resolution, but the very same considerations apply to data sequences sampled in space. Whether analyzing spatial or temporal behaviors, the power spectrum allows us to identify specific scales or ranges of scales which dominate the spatiotemporal behavior of the signaling network being observed.

4.1.3 Optimizing the spatiotemporal sampling of activity fluctuations—As mentioned above, the accurate measurement of the topology and kinetics of information flow in signaling networks requires sampling of the associated activities at appropriate spatiotemporal scales. These scales are rarely known prior to the experimental process and it is therefore necessary to estimate them from measurements of the signaling system of interest. We describe here how the ACF and power spectrum support this scale selection.

The former is a time domain method that estimates the overall memory of the system that generated the time series whereas the power spectrum shows the combination of frequencies or frequency bands that compose the signal. For activity biosensor movies, it is generally easier to consistently estimate the ACF than the power spectrum. This is because a reliable estimation of the power spectrum requires the acquisition of longer time series (Box et al., 1994). Yet, both techniques can assist in identifying the sampling rate required for the reconstruction of signaling events. In general, this involves iterating between experiment and estimation of the ACF and power spectrum until certain requirements are met. For instance, starting with an image acquisition rate F_0, one can estimate the autocorrelation of the sampled signals and record the maximum significant lag $\tau_{\max}$. To test whether F_0 is sufficient, one can estimate the autocorrelation using a down-sampled version of the signals, where for example every other frame is excluded from the analysis. If the maximum lag τ_{max}^{down} of the down-sampled signal has the same value as $\tau_{\max}$, then the current sampling rate F_0 is more than sufficient, and can be decreased to reduce image acquisition artifacts such as phototoxicity or photobleaching. However, if the new maximum lag τ_{max}^{down} is smaller than $\tau_{\max}$, no conclusions can be drawn about the sufficiency of F_0. A new experiment with a faster frame rate F_1 needs to be performed. Once again, the ACF and the maximum lag τ_{max}' associated with the new frame rate F_1 need to be estimated and compared with $\tau_{\max}$. Similarly to the previous comparison, F_1 over-samples the signals if $\tau_{max}'=\tau_{max}$ but no conclusions can be drawn if $\tau_{max}'>\tau_{max}$. New experiments with faster frame rates are needed until the condition $\tau_{max}'=\tau_{max}$ is satisfied. The satisfaction of this over-sampling condition implicitly translates into compliance with the Nyquist theorem. Similarly, the power spectrum can also be used to elucidate the necessary spatiotemporal sampling scales. Starting with an under-sampled signal, gradual increases in the frame rate should result in increasing amplitudes in higher frequency bands of the power spectrum. This is because higher acquisition rates allow measurement of fluctuations associated with high-frequency signaling behaviors. Over-sample conditions are reached when an increase in the sampling rate does not result in additional significant amplitudes in the power spectrum. This indicates that the highest-frequency signaling behaviors have already been captured, and faster imaging will provide little additional information.

The same procedures described above can be applied to the spatial component of the sampled signals. Here, the analysis needs to determine first whether the image pixel size is sufficiently small to capture the spatial variation of the observed signaling activity. If this is not the case, then the imaging setup must be modified by either an increase in magnification and/or decrease in camera pixel size. If however the pixel size is sufficiently small, the spatial autocorrelation function or power spectrum can be used to determine the allowable spatial binning of the signal, *i.e.* the size of the sampling windows. For FRET-based biosensors utilization of immersion objectives is usually necessary to collect the weak fluorescence signal these probes emit. Immersion objectives have a magnification of 40× and more, which implies sub-micron pixel sizes (depending on the camera). Considering the range of diffusion rates of signaling molecules in cells, this is generally sufficient for the sampling of signaling events. Hence, the spatial scale analysis is generally limited to

defining the appropriate binning of an inherently oversampled signal into sampling windows.

Figure 4 shows an example of the effects of the chosen sampling rate on the reconstruction of a theoretical signal. The simulated signal used in this example has two frequency bands [0.009–0.01] Hz and [0.04–0.05] Hz with lower amplitude values for the second band. In Figure 4, both autocorrelation and power spectrum were calculated by sampling the original signal every 5, 10 and 20 seconds (or 0.2, 0.1 and 0.05 Hz). The immediate decay of the autocorrelation function to an insignificant value in Figure 4**B** would suggest a short memory in this time series. However, the power spectrum in 4**C** clearly shows information in the 0.009–0.01 Hz frequency band. This example illustrates two key properties of the time scale analysis via ACF and power spectrum. First, per the Nyquist theorem, at a sampling rate of 0.05 Hz no signal faster than 0.025 Hz can be reconstructed. Therefore, the sampling in this example is insufficient for a complete recovery of the full information contained in the signal. Second, while the computation of the autocorrelation function is more robust for short time series, the power spectrum can recover partial information about the signal (only the first frequency band of the signal was recovered in Figure 4**C**). Following the logic introduced above for optimizing the time sampling, increasing the sampling frequency to 0.1 Hz results in both a more informative ACF and power spectrum (Figure 4 **E, F**) although the power spectrum still can not fully resolve the entire range of frequencies in the signal. A further increase to 0.2 Hz does not change the maximum lag in the autocorrelation (Figure 4 **H**), indicating 0.2 Hz as a reliable frequency for reconstruction of the original signal, and allowing complete reconstruction of the signal's frequency components in the power spectrum. This illustrates how, even without *a priori* knowledge of the spatiotemporal scales over which a signaling network operates, iteration between experiment and analysis needs to be implemented for selection of the appropriate sampling scales.

4.2 Establishing relationships between pathway events

The ACF and power spectrum are valuable tools for understanding the dynamics of a signal and therefore a single component of a signaling network. However, much of the functionality of a biological system relies on the interactions among their constituents. We introduce here two statistical tools that can be used for uncovering relationships between measured signals and thereby allow inference of the nature of interactions between the measured signaling components: the cross-correlation and coherence. Analogous to how the ACF and power spectrum measure the relationship between a signal and itself at different time delays or frequencies, the cross-correlation function (CCF) and coherence quantify linear relationships between two different signals in the time and frequency domain, respectively. Combining these with spatially localized sampling, the relationship among signal events can be probed for different cellular regions.

4.2.1 Cross-correlation—Analogous to the ACF, the CCF determines the strength of any linear relationship between *two* sampled time series representing two different signaling activities as a function of a given lag τ (Box et al., 1994). One can think of the lag in the following way: a positive lag means that one time series is fixed as the reference and the second time series is shifted into the past, *i.e.* the events in the second time series happen

after the potentially corresponding events in the reference series. With a negative lag, the second time series is shifted into the future, *i.e.* the events in the second time series happen before the potentially corresponding events in the reference series. The cross correlation value for a particular τ indicates how strong the similarity of the two time series is at that particular lag. Unless the two time series are identical or symmetric, the cross-correlation function is not symmetric about $\tau = 0$. Once the CCF is computed, the key question is whether the magnitude of the function maximum is statistically significant. The cross-correlation between two signals *X* and *Y* is considered significant if it exceeds for at least one time lag τ the CCF of two uncorrelated random signals with the same variance and number of points as in *X* and *Y*. Among several mechanisms, a likely explanation for a significant positive cross-correlation could be that the events of one time series partially activate the events of the second time series. Conversely, a significant negative magnitude likely indicates that the events of one time series inhibit events of the second time series. Although cross-correlation is not a strictly causative measure (Vilela and Danuser, 2011) the time lag associated with the CCF maximum defines which of the two time series happens, on average, first, suggesting upstream – downstream relations between the activities. Thus, the CCF provides insight not only of the strength and nature of the relationship between two signaling activities, but also predicts the temporal organization and kinetics of this relationship.

4.2.2 Coherence—Complementary to the cross-correlation, the coherence is a measure of the relationship of two signals in the frequency domain (Brillinger and Krishnaiah, 1983). Mathematically, it is defined as the Fourier transform of the cross-correlation. The coherence quantifies the overall linear coupling of two time series as a function of the specific frequencies or frequency bands shared between them. Because of this selectivity of shared frequencies, the coherence can resolve situations where one signaling activity relates to multiple other signaling activities, but at different frequency bands(Brillinger and Krishnaiah, 1983).

Figure 5 illustrates the use of cross-correlation and coherence for characterizing the relationship between two hypothetical activities *X* and *Y*. Panel A shows the two time series and how their information is transmitted through a **communication channel** (Feinstein, 1958). The cross-correlation and coherence analyses serve the purpose of identifying whether there is any linear information flow between *X* and *Y* through the channel. In a cellular context, this communication channel conceptualizes the cascade of physicochemical events that link the activation/deactivation of one particular signal to the activation/ deactivation of another signal. Dependent on the kinetics and the complexity of this event cascade, the information transfer between the signals may lead to more or less delay, which is decoded by the time lag τ of the dominating cross-correlation maximum or minimum. Also, in the absence of strong feedback, the sign of the time lag indicates the directionality of information flow. As illustrated in Fig. 5C, the coherence informs us about the frequencies that are transmitted through the channel. Importantly, frequency and time delay are not equivalent. Two particular signals may be coupled through distinct frequency bands but both bands may have the same time lag because the molecular processes underlying the information flow obey the same overall kinetics. On the other hand, one particular signal

may communicate with two other signals in the same frequency band but with different time lags.

4.3 Integrating results: Averaging over multiple windows and cells

We have described in the previous sections statistical tools that allow the analysis of a single time series or a pair of time series extracted from one local sampling window of a biosensor dataset. However, the data from an individual sampling window are very noisy. Therefore, correlation, power spectra, and coherence measurements must be averaged over multiple windows and over multiple cells. Averaging these metrics requires some caution as simple mean values may be biased due to a relatively small number of potentially non-normally distributed data points. Here, we illustrate the use of the bootstrap technique to allow accurate averaging. This technique generates a large number of samples by randomly resampling the existing data with replacement (Zoubir and Iskander, 2004). For more robust results, variance stabilization methods can be added (Zoubir and Iskander, 2004). Figure 6 shows a mean ACF bootstrapped from the time series of different sampling windows in a mouse embryonic fibroblast (MEF) expressing a FRET-based activity biosensor of the small GTPase Rac1 (Machacek et al., 2009). First, the autocorrelation for time series extracted at individual windows is calculated. Then the bootstrap algorithm samples with replacement the autocorrelation values from all windows for a given lag to estimate one final value with a confidence interval. This process is repeated for all lags resulting in a global autocorrelation function for the entire cell.

The same approach can be taken to compute an average cross-correlation function between two activities. Importantly, the data entering the bootstrap can originate from windows in a single or multiple cells. The fundamental assumption underlying the analysis is that although each of these windows generates a random fluctuation series, their statistical properties are conserved between windows and between cells. Practically, this means that data from windows with similar properties are integrated, *e.g.* from all windows at the boundary of moving cell edges, or from all windows at the boundary of quiescent cell edges, or from all windows 5 microns from the cell edge. How these windows are categorized varies with the specific application and research question. Given these assumptions, the bootstrap allows accurate aggregation of results across cells and cell regions, increasing the statistical power of these results and the generality of their biological implications.

4.4 Integrating results: Multiplexing of different activities using a common fiduciary

Current biosensor designs and imaging technology do not allow the simultaneous observation of more than two, or maximally three, molecular activities in living cells at sufficient spatiotemporal resolution (Hodgson et al., 2008; Welch et al., 2011). However, the goal of these live cell fluctuation studies is to reconstruct the flow of information in pathways with tens of components. To achieve this goal, fluctuation data of different biosensors imaged separately in different experiments must be integrated *in silico*. We refer to this approach as computational multiplexing (Welch et al., 2011). To allow computational multiplexing, two important requirements need to be fulfilled. First, identical experimental conditions must be maintained across all experiments. Second, each experiment must measure one activity which is common to at least one other experiment. This common

activity shared between experiments provides a reference or 'fiduciary', allowing the time series from different experiments to be linked (Machacek et al., 2009; Welch et al., 2011). The simplest strategy for computational multiplexing is to relate all experimental data to a single common fiduciary across all experiments. This strategy was established for the first time by Machacek et al. (Machacek et al., 2009) where the cell edge velocity was exploited to characterize the coordination of the small GTPases Rac1, RhoA and Cdc42 during cell protrusion. Basal fluctuations of these signaling molecules were measured over time in the context of cells undergoing directed migration. Each experiment imaged the activity of one GTPase at the time. Based on the cross-correlation analysis between biosensor activity and cell edge velocity the timing of each one of the GTPases relative to the onset of protrusion was identified. This alignment of GTPase activity and cell edge motion indirectly made predictions as to how the GTPases would be timed (and spatially shifted) relative to one another. These predictions were then confirmed in experiments where two spectrally orthogonal biosensors were imaged concurrently (Machacek et al., 2009). Thus by exploiting a fiduciary common to several experiments, computational multiplexing allows us to infer the flow of information in signaling networks with many more components than can be observed in one experiment.

4.5 Integrating results: Comparing correlation and coherence data between different subcellular locations

The propagation of signaling events is organized not only in time but probably also in space. Here we give a glimpse of how local sampling of biosensor activity fluctuations in small windows can be exploited to test this notion. We demonstrate the variation in the relation between the activity of the small GTPase Rac1 and cell edge motion at various distances from the cell boundary. Rac1 is thought to activate the formation of protruding lamellipodia (Raftopoulou and Hall, 2004). Thus, it would be expected that signaling information would flow from Rac1 activation to cell edge protrusion. Furthermore, this relationship would be expected to taper off rapidly with increasing distance from the protruding edge. Figure 7 shows Rac1 activity sampled in 45 windows at the cell boundary (A) and in 45 windows 2 microns away from the cell edge (B). For the windows at the cell edge velocity values of the local cell edge motion are sampled as well (C). Both cross-correlation and coherence reveal a stronger interaction between the cell edge velocity and Rac1 activity sampled 2 microns away from the cell edge. The time lag of the cross correlation peak indicates that Rac1 is activated, on average, ~40 seconds after the increase in cell edge velocity. The cross-correlation peak for windows at the cell edge is weaker than for those at 2 microns distance and the time shift between edge motion and Rac1 activation increases. These fundamentally distinct behaviors of Rac1 at the cell edge versus further away from it are corroborated by distinct bands of significant coherence. At 2 microns from the cell edge the coherence peaks at 0.01 Hz, or in a cycle of 100 seconds. This cycle time coincides with the ~100 s period of the protrusion/retraction cycles in these cells, suggesting that Rac1 activity at 2 microns from the edge is part of a feedback mechanism that links edge motion to the reactivation of GTPase signals away from the cell edge, probably in maturing adhesions. The coherence function at the cell edge covers a wider range of frequencies. This indicates that activation of Rac1 at these distances is more random and not directly related to the protrusion/ retraction cycle. Current work in our labs is focused on investigating the molecular

differences between these different regimes of Rac1 regulation. This example highlights how the combination of the approaches described in this chapter can provide unprecedented understanding of the dynamics and variability of signal transduction with sub-cellular resolution.

5. Outlook

We present in this chapter the basic concepts of using fluctuations in signaling activity as measured by biosensors for the reconstruction of information flows in signaling networks. Autocorrelation and power spectral analyses can characterize the spatiotemporal properties of individual signaling components, and coherence and cross-correlation provide a measure of the relationships between different signaling components. Furthermore, in combination with an experimental fiduciary, methods like cross-correlation and coherence can be used to computationally multiplex data from different experiments in pathway models that consider many more components than can be observed directly in a single experiment. Although informative, these basic, linear statistical methods are unable to uncover more complex relationships among signaling components such as feedback loops. In order to clarify such interaction, we foresee the use of more sophisticated tools that can further decompose the link between two signals and probe the possibility of bi-directional information flow. Some tools from the fields of economics and neuroscience possess this capability; however a substantial effort is still necessary to adopt these tools to biosensor fluctuation data.

Acknowledgments

References

Abdul-Manan N, Aghazadeh B, Liu G, Majumdar A, Ouerfelli O, Siminovitch K, Rosen M. Structure of Cdc42 in complex with the GTPase-binding domain of the ';Wiskott-Aldrich syndrome'; protein. Nature. 1999; 399:379–462. [PubMed: 10360578]

Berg J, Hung Y, Yellen G. A genetically encoded fluorescent reporter of ATP:ADP ratio. Nature methods. 2009; 6:161–167. [PubMed: 19122669]

Bosgraaf L, van Haastert PJ, Bretschneider T. Analysis of cell movement by simultaneous quantification of local membrane displacement and fluorescent intensities using Quimp2. Cell motility and the cytoskeleton. 2009; 66:156–165. [PubMed: 19206151]

Box, GEP.; Jenkins, GM.; Reinsel, GC. Time series analysis : forecasting and control. 3rd ed.. Prentice Hall: Upper Saddle River NJ.; 1994.

Brigham, EO. The fast Fourier transform and its applications. Prentice Hall: Englewood Cliffs N.J.; 1988.

Brillinger, DR.; Krishnaiah, PR. Time series in the frequency domain. North-Holland Amsterdam: 1983.

Burridge K, Wennerberg K. Rho and Rac take center stage. Cell. 2004; 116:167–179. [PubMed: 14744429]

Digman M, Gratton E. Lessons in fluctuation correlation spectroscopy. Annual review of physical chemistry. 2011; 62:645–713.

Feinstein, A. Foundations of information theory. New York: McGraw-Hill; 1958.

Goldman, RD.; Swedlow, J.; Spector, DL. Live cell imaging : a laboratory manual. 2nd ed.. Cold Spring Harbor N.Y.: Cold Spring Harbor Laboratory Press; 2010.

Hodgson L, Pertz O, Hahn KM. Design and optimization of genetically encoded fluorescent biosensors: GTPase biosensors. Methods in cell biology. 2008; 85:63–81. [PubMed: 18155459]

Ji L, Lim J, Danuser G. Fluctuations of intracellular forces during cell protrusion. Nature cell biology. 2008; 10:1393–U1338.

Lim JI, Sabouri-Ghomi M, Machacek M, Waterman CM, Danuser G. Protrusion and actin assembly are coupled to the organization of lamellar contractile structures. Experimental cell research. 2010; 316:2027–2041. [PubMed: 20406634]

Machacek M, Danuser G. Morphodynamic profiling of protrusion phenotypes. Biophysical journal. 2006; 90:1439–1452. [PubMed: 16326902]

Machacek M, Hodgson L, Welch C, Elliott H, Pertz O, Nalbant P, Abell A, Johnson GL, Hahn KM, Danuser G. Coordination of Rho GTPase activities during cell protrusion. Nature. 2009; 461:99–103. [PubMed: 19693013]

Nalbant P, Hodgson L, Kraynov V, Toutchkine A, Hahn K. Activation of endogenous Cdc42 visualized in living cells. Science. 2004; 305:1615–1624. [PubMed: 15361624]

Newman RH, Fosbrink MD, Zhang J. Genetically Encodable Fluorescent Biosensors for Tracking Signaling Dynamics in Living Cells. Chemical Reviews. 2011; 111:3614–3666. [PubMed: 21456512]

Periasamy A. Fluorescence resonance energy transfer microscopy: a mini review. Journal of biomedical optics. 2001; 6:287–378. [PubMed: 11516318]

Pertz O, Hodgson L, Klemke R, Hahn K. Spatiotemporal dynamics of RhoA activity in migrating cells. Nature. 2006; 440:1069–1141. [PubMed: 16547516]

Raftopoulou M, Hall A. Cell migration: Rho GTPases lead the way. Developmental Biology. 2004; 265:23–32. [PubMed: 14697350]

Schwille P, Haustein E. Fluorescence correlation spectroscopy : An introduction to its concepts and applications. Spectroscopy. 2009; 94:1–34.

Slavík, J. Fluorescence microscopy and fluorescent probes. New York: Plenum Press; 1996.

Tkachenko E, Sabouri-Ghomi M, Pertz O, Kim C, Gutierrez E, Machacek M, Groisman A, Danuser G, Ginsberg MH. Protein kinase A governs a RhoA-RhoGDI protrusion-retraction pacemaker in migrating cells. Nature cell biology. 2011; 13:660–667.

Tyson R, Epstein D, Anderson K, Bretschneider T. High Resolution Tracking of Cell Membrane Dynamics in Moving Cells: an Electrifying Approach. Mathematical Modelling of Natural Phenomena. 2010; 5:34–89.

VanEngelenburg SB, Palmer AE. Fluorescent biosensors of protein function. Curr Opin Chem Biol. 2008; 12:60–65. [PubMed: 18282482]

Vilela M, Danuser G. What's wrong with correlative experiments? Nature cell biology. 2011; 13:1011.

Waterman-Storer C, Desai A, Bulinski J, Salmon E. Fluorescent speckle microscopy, a method to visualize the dynamics of protein assemblies in living cells. Current biology. 1998; 8:1227–1257. [PubMed: 9811609]

Welch CM, Elliott H, Danuser G, Hahn KM. Imaging the coordination of multiple signalling activities in living cells. Nature reviews. Molecular cell biology. 2011; 12:749–756. [PubMed: 22016058]

Zoubir, AM.; Iskander, DR. Bootstrap techniques for signal processing. Cambridge, Cambridge: 2004.

NIH-PA Author Manuscript

NIH-PA Author Manuscript
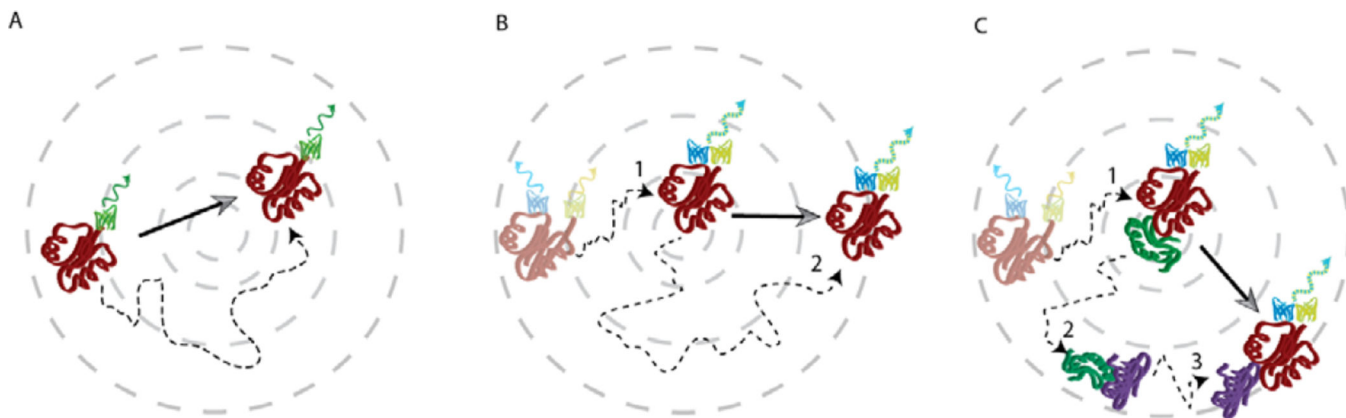
NIH-PA Author Manuscript

Figure 1. Protein translocation versus spatial propagation of protein signals
Protein translocation is illustrated by dotted arrows, and measured signal propagation by solid arrows. In **A,** a fluorescently-tagged molecule diffuses in space. The fluorescent signal only reports the translocation of the molecule. **B** and **C** show two different mechanisms for the spatial propagation of signals. In **B**, an initially inactive signaling molecule is activated (step 1). The activation state is monitored by a biosensor, in this example a FRET-based sensor, that reads out conformational changes associated with a state switch of the signaling molecule. In this scenario, the signal is transmitted by physical translocation of the activated molecule by diffusion (step 2). In **C**, activation of the signaling molecule (step 1) promotes transient binding of an effector (green), which diffuses and activates a second intermediary molecule (purple, step 2). The latter then binds and activates another signaling molecule of the first kind (step 3). This leads to signal propagation in space which differs from the translocation of the biosensor.
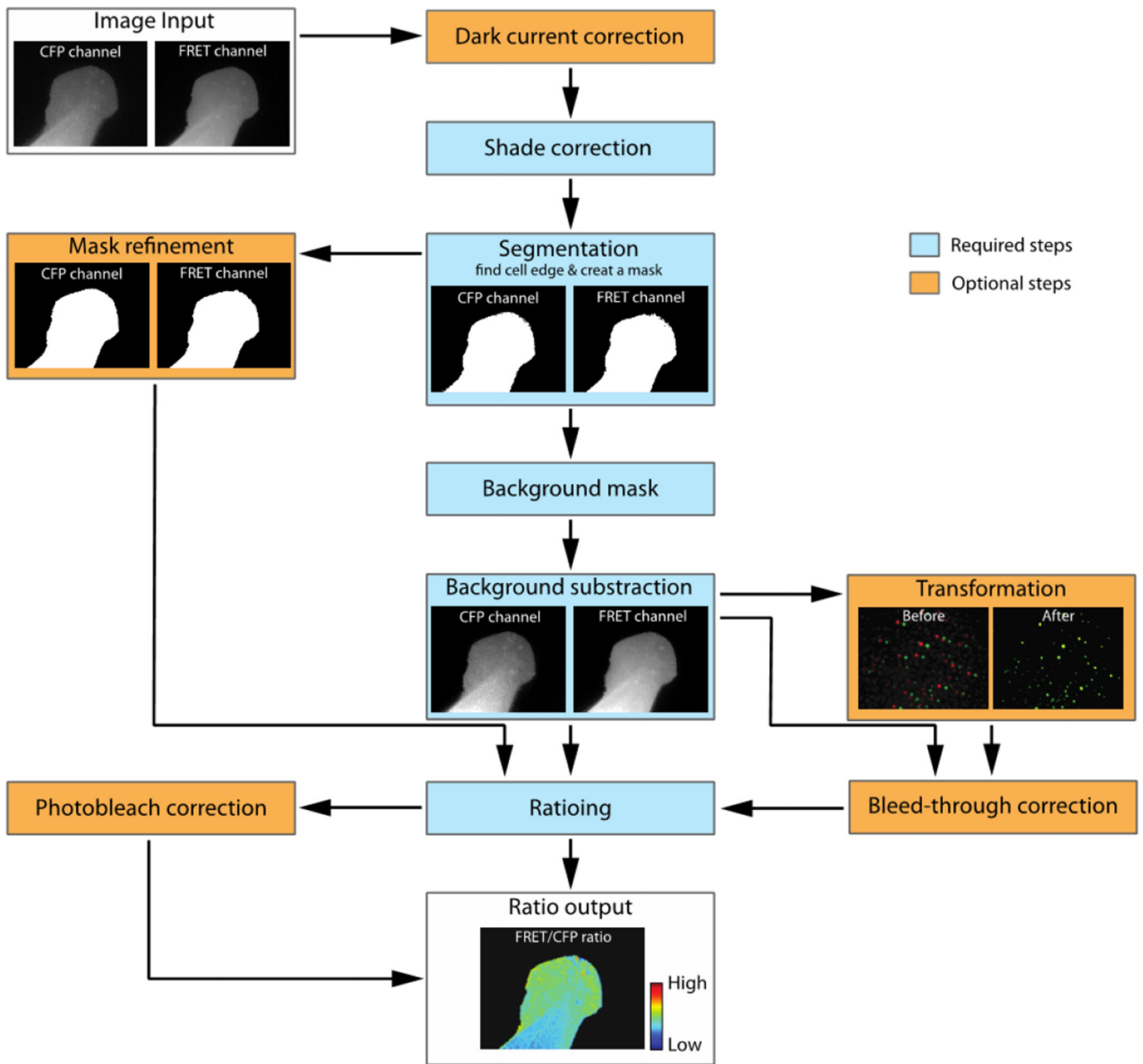
Figure 2. Image corrections and processing required for FRET-based biosensor readouts of signaling activities

The end product of the workflow is a ratio image that indicates the spatial biosensor activity at each frame of the movie.
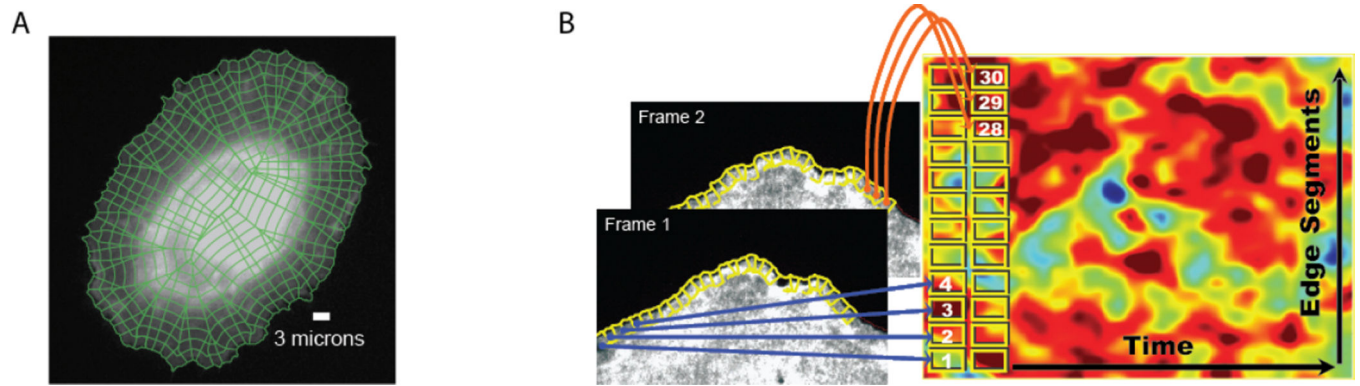
Figure 3. Windowing process

A, Segmentation of a cell into sampling windows. **B**, Sampling of the fluorescence signal and construction of the spatiotemporal activity map. Figure is reproduced, with permission, from references (Lim et al., 2010; Welch et al., 2011).
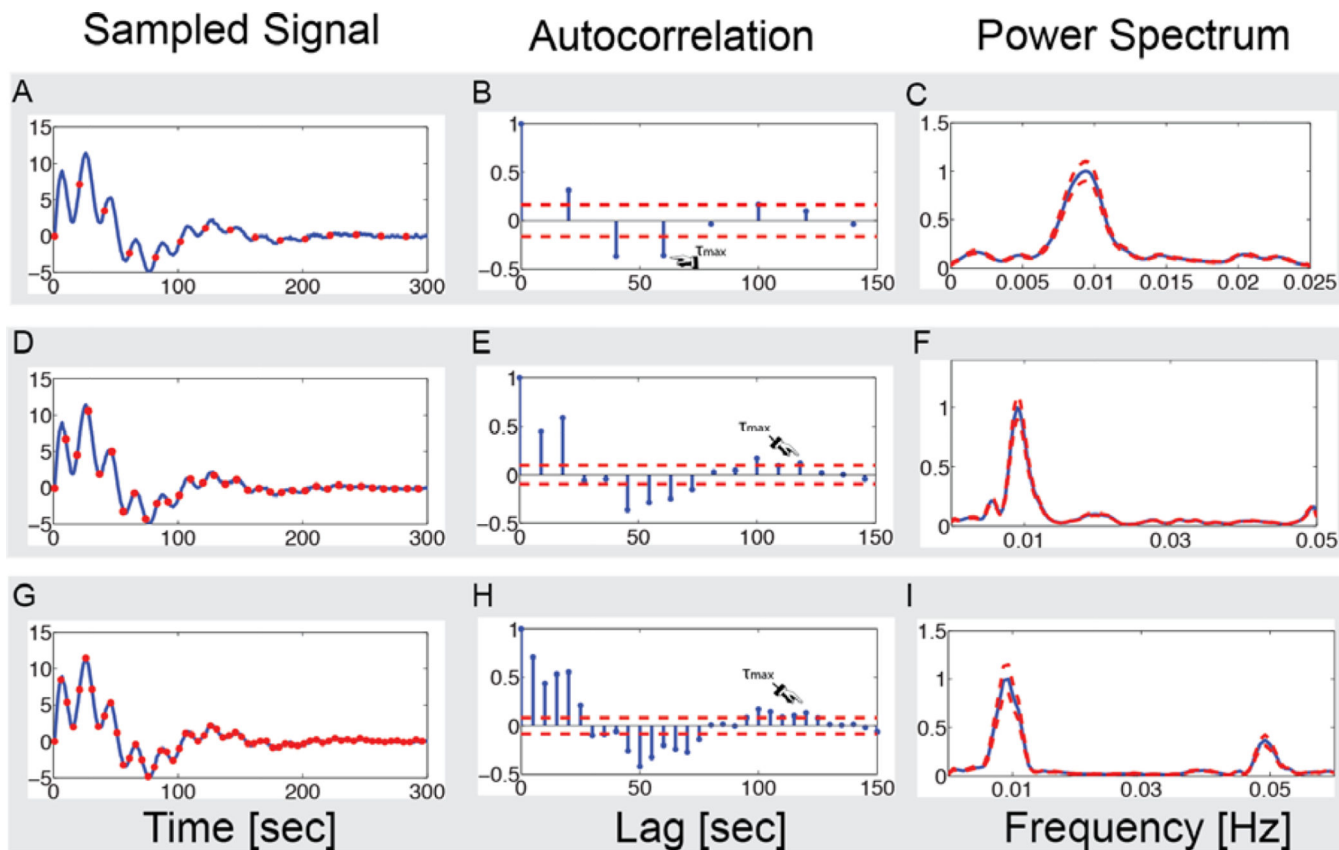
Figure 4. Sampling effects in the autocorrelation and power spectrum
The first column [**A, D** and **G**] shows the continuous signal (in blue) and the signal samples (in red) used to calculate the autocorrelation and power spectrum. The second column [**B, E** and **H**] shows their autocorrelation functions. The red dashed lines indicate the 95% confidence level of autocorrelation values. The third column [**C, F** and **I**] illustrates the power spectrum. The red dashed lines indicate the confidence interval with p-value of 0.05. The confidence interval in this case indicates the precision of the power spectrum estimation.
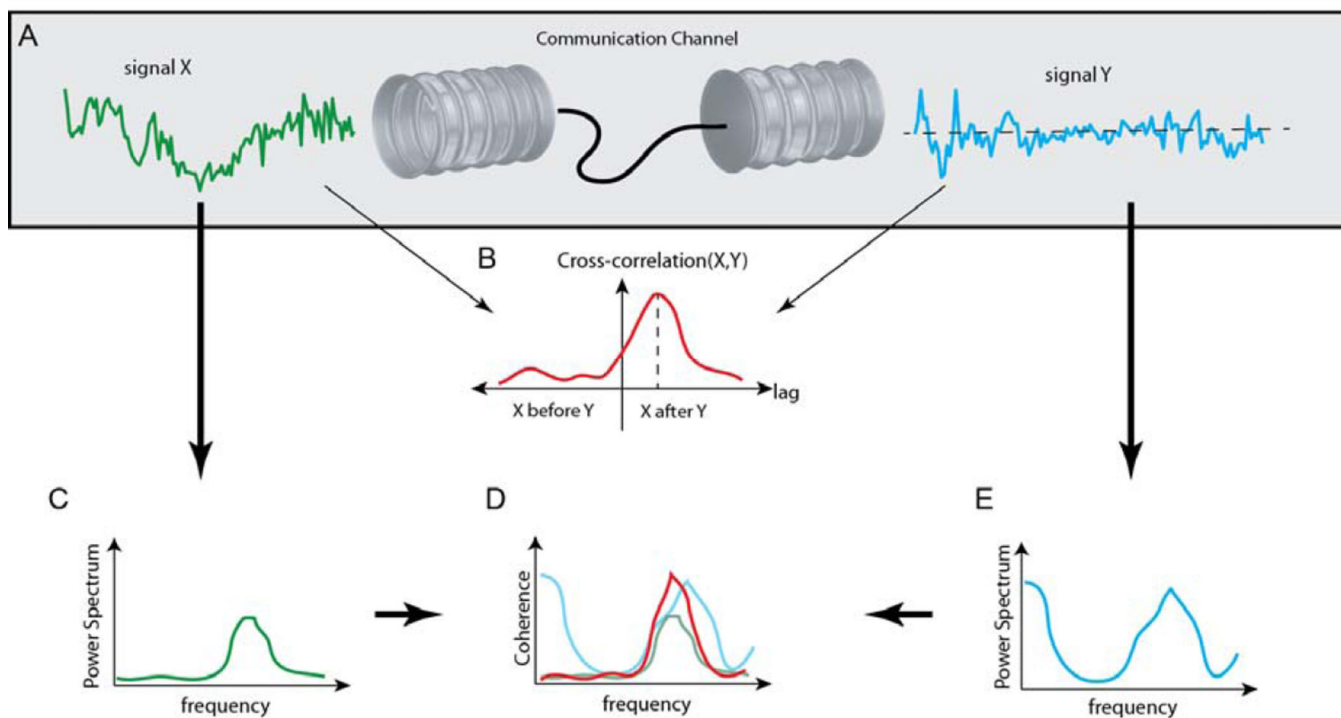
Figure 5. Characterization of information flow between two activities *X* and *Y* through a communication channel

A, the communication channel conceptualizes the cascade of molecular events that is triggered by one of the activities and contributes to the modulation of the other activity. **B**, cross-correlation between the activities. Here, activity *Y* is used as the reference. Accordingly, the positive time lag of the peak correlation value suggests that the fluctuations in activity *Y* lags those of activity *X*, leading to prediction that *X* may be upstream of *Y*. **C–E**, coherence analysis. Panels C and E show the power spectra of the two activities. Panel D illustrates that the coherence (in red) represents the overlap of the two spectra.
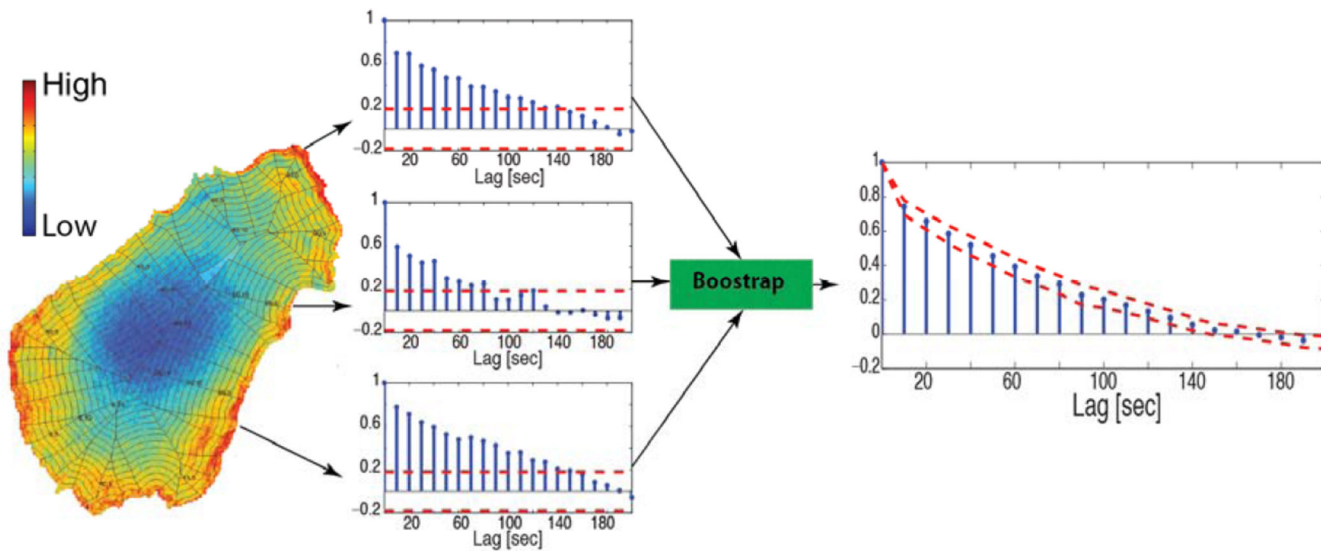
Figure 6. Bootstrap method to extract an average autocorrelation function of a molecular activity (in this example Rac1 activation) sampled in all windows along the cell edge
The autocorrelation is first calculated for time series in individual windows. In the sampling process, values of the autocorrelation that fall inside the confidence bounds (red dashed lines) are set to zero. A 95% confidence interval is estimated for each value of the bootstrapped autocorrelation based on the empirical distribution built by the algorithm.
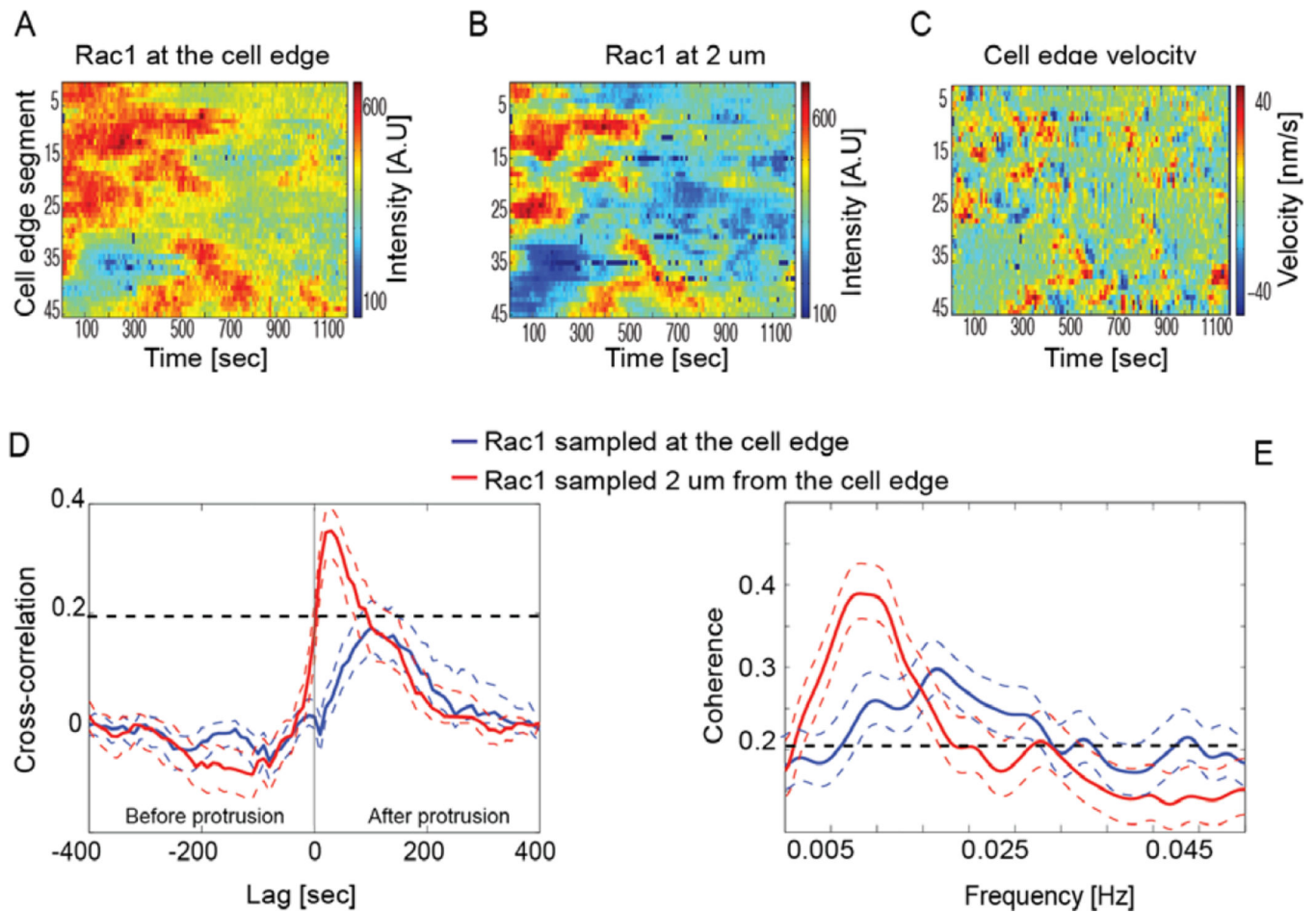
Figure 7. Spatial variation of the relationship between cell edge velocity and Rac1 signaling sampled at different distances from the cell edge

A–B, spatiotenmporal activity maps of Rac1 signaling sampled at the cell edge and 2 microns inwards, respectively. **C**, cell edge velocity map. **D–E**, cross-correlation (with edge velocity as reference) and coherence between the cell edge velocity and Rac1 activation sampled at the edge and 2 microns inwards.